UNIVERSITY OF LEEDS

This is a repository copy of *Influence of charge status on the stress safety properties of Li(Ni⅓Co⅓Mn⅓)O₂ cells*.

White Rose Research Online URL for this paper:
http://eprints.whiterose.ac.uk/104503/

Version: Accepted Version

Article:
Zhou, S, Wang, G, Xiao, Y et al. (3 more authors) (2016) Influence of charge status on the stress safety properties of Li(Ni⅓Co⅓Mn⅓)O₂ cells. RSC Advances, 6 (68). pp. 63378-63389. ISSN 2046-2069

https://doi.org/10.1039/c6ra08774d

(c) 2016, RSC. This is an author produced version of a paper published in RSC Advances. Uploaded in accordance with the publisher's self-archiving policy.

Reuse
Unless indicated otherwise, fulltext items are protected by copyright with all rights reserved. The copyright exception in section 29 of the Copyright, Designs and Patents Act 1988 allows the making of a single copy solely for the purpose of non-commercial research or private study within the limits of fair dealing. The publisher or other rights-holder may allow further reproduction and re-use of this version - refer to the White Rose Research Online record for this item. Where records identify the publisher as the copyright holder, users can verify any specific terms of use on the publisher's website.

Takedown
If you consider content in White Rose Research Online to be in breach of UK law, please notify us by emailing eprints@whiterose.ac.uk including the URL of the record and the reason for the withdrawal request.

White Rose university consortium
Universities of Leeds, Sheffield & York

eprints@whiterose.ac.uk
https://eprints.whiterose.ac.uk/

View Article Online
DOI: 10.1039/C6RA08774D

Influence of charge status on the stress safety properties of $Li(Ni_{1/3}Co_{1/3}Mn_{1/3})O_2$ cells

Shuo Zhou [1], Guixin Wang [1,*], Yao Xiao [1], Qian Li [1], Dongmin Yang [2], Kangping Yan [1]

[1] *College of Chemical Engineering, Sichuan University, Chengdu 610065, China*

[2] *School of Civil Engineering, University of Leeds, LS2 9JT, Leeds, UK*

ABSTRACT

In order to improve the safety management, the stress changes of $Li(Ni_{1/3}Co_{1/3}Mn_{1/3})O_2$ (NMC) cells are real-time monitored using non-destructive strain gauges, and the effects of gauge substrate, temperature and state-of-charge (SOC) have been investigated. The shell exhibits elastic deformation behaviour, and the strain-stress relationship is established. As the temperature increases from 25 to 80 ºC, the stress of the NMC cells increases from 0 to 275 MPa, especially greatly at 70 °C and sharply at 80 ºC after 18 h. The stress increases from 0 to 9.2 MPa when the potential increases from 2.8 to 4.3 V. However, the value rises from 10 to 55 MPa when the voltage increases from 4.6 to 5.0 V during overcharge process; while an obvious increase of stress appears when the cut-off voltage is below 0.6 V during over-discharge tests. The facile method is significant for the non-destructive inspection and emergency management of batteries.

Keywords: Mechanical analysis; Real-time monitoring; $Li(Ni_{1/3}Co_{1/3}Mn_{1/3})O_2$; State of charge; Temperature effects

* Corresponding author.
E-mail: guixin66@scu.edu.cn, guixinwang1@gmail.com, Tel: 86-28-85467527;

Published on 22 June 2016. Downloaded by Sichuan University on 24/06/2016 05:17:58.

RSC Advances Accepted Manuscript

View Article Online
DOI: 10.1039/C6RA08774D

Published on 22 June 2016. Downloaded by Sichuan University on 24/06/2016 05:17:58.

1. Introduction

Continuous environmental deterioration and traditional fossil fuel resource depletion make (hybrid) electric vehicles highly attractive for city transport. As one of their key power sources, lithium-ion batteries have gained tremendous attentions because of their unique advantages such as high energy density, low weight and high environmental compatibility. However, the safety issues, especially swelling, leakage, burning and explosion, restrict their sustainable and fast development as well as large scale applications. Such typical hazards usually take place when the maximum inner stress is higher than the strength of the outer shell and could cause the severe damage on the whole battery. Therefore, it is vital and essential to monitor the stress changes and take precaution of the potential dangers for the safety management of batteries. A few methods have been reported to investigate the stress changes in batteries, with a focus on the stress of the microscale particles in the active materials [1,2] and the safety simulation of the shell of battery [3,4]. However, the typical safety issues are directly related to the macroscopic stress in a battery shell, which has not yet been carefully considered. Such macroscopic stress, including the stress of particles and other stresses, is highly complex as a result of the interaction between particles, thermal expansion, interaction between electrode and electrolyte, electrochemical reaction, and so on. Actually, a battery is a sealed can with a thin shell, of which the inner pressure can be tested via the outer surface. A mechanical strain gauge (or strain gage) is a useful device to accurately measure the pressure/stress via the small changes in electrical resistance of wire grids under strain. If the battery shell is under linear elastic deformation, the strains measured by the strain gauge on the shell surface without destruction can be used to determine the macroscopic stress of batteries according to the Hooke's law.

As one of the popular cathode materials with high mass density, NMC can meet the requirements of pulse power characteristics for transport applications in a small volume, but the safety problems

RSC Advances Accepted Manuscript

View Article Online
DOI: 10.1039/C6RA08774D

Published on 22 June 2016. Downloaded by Sichuan University on 24/06/2016 05:17:58.

(especially large deformations and/or leakage due to abuse or elevated temperature) hamper its extensive applications [5,6]. Various studies of NMC have been reported, attempting to understand and solve these problems. For example, the thermal stability of charged NMC [7] and the gas generation of $Li_4Ti_5O_{12}$/NMC cells at 80 °C [8] have been investigated. The production of heat and gas can cause runaway reactions and trigger explosion of batteries [9], which will be very hazardous under abnormal operating conditions [10]. According to the production processes, such problems would result in the large deformations and then leakage of batteries. If the stresses that are closely related to the deformations of the battery surface can be monitored and corresponding measures can be taken in advance, the hazards like leakage, burning or explosion could be efficiently prevented. Therefore, it is necessary to monitor the macroscopic stress changes of NMC batteries in order to develop further measures for safe applications.

In this paper, strain gauges are adopted to real-time monitor the strains and stresses of $Li(Ni_{1/3}Co_{1/3}Mn_{1/3})O_2$ lithium ion cells under various conditions. The reliability of the monitoring tests, along with the relationship between macroscopic mechanical stress and electrochemical performance, has been analysed. The reasons for such stress changes have also been discussed.

2. Experimental

2.1. Synthesis of NMC

Powders of $(Ni_{1/3}Co_{1/3}Mn_{1/3})(OH)_2$ and $LiOH{\cdot}H_2O$ (molar ratio of 1:1.05) were fully mixed to form a rheological precursor using alcohol as the dispersing agent by a planetary ball milling at 180 rpm for 4 h. The milled precursor was preheated at 550 °C in air for 4 h in a muffle oven and further calcined at 750~850 °C in air for 12 h. The as-synthesized black product was ground for physicochemical characterization and stress tests.

RSC Advances Accepted Manuscript

View Article Online
DOI: 10.1039/C6RA08774D

Published on 22 June 2016. Downloaded by Sichuan University on 24/06/2016 05:17:58.

2.2. Physicochemical characterization

In order to eliminate the unexpected influence of anode materials, common lithium cells composed of NMC and lithium metal are chosen for stresses and strains monitoring tests under different conditions. The as-synthesized powder sample for electrochemical characterization was well mixed with 10 wt.% of conductive additive of super P and 7 wt.% of commercial PVDF binder to form a homogeneous viscous slurry to coat a cleaned aluminium foil using a doctor blade. After being dried at 100 ℃, the aluminium foils loaded with active materials were cut into 1.2 cm^2 wafers which were further dried at 100 ℃ under vacuum for 12 h before being used as the working electrodes. Using pure lithium metal as the counter and reference electrodes, CR2032 coin cells were assembled in an argon-filled glove box by sandwiching a Celgard 2300 microporous separator between the working electrode and lithium disc. The electrolyte was 1 M $LiPF_6$ in a mixture of ethyl carbonate (EC), dimethyl carbonate (DMC) and ethyl methyl carbonate (EMC) (1:1:1 in vol., Shenzhen Capchem Chemicals Co. Ltd., China).

Galvanostatic charge/discharge cycling tests of the above devices were carried out with different potential windows, current rates and working temperatures on a Neware battery-testing instrument (Shenzhen Neware Technology Ltd., China). Electrochemical Impedance Spectroscopy (EIS) measurements were conducted before and after stress tests under different conditions in the frequency range from 100 kHz to 0.01 Hz with a sinusoidal excitation voltage of 10 mV, and the impedance curves were fitted using Zsimpwin and Zview softwares. Cyclic voltammetry (CV) technique was used in the voltage window of 2.8 ~ 4.3 V to investigate the electrode reaction process after different cycles. Both EIS and CV tests were carried out on an electrochemical workstation consisting of a PAR 273A potentiostat/galvanostat and a signal recovery model 5210 lock-in-amplifier controlled by a Powersuit software (Princeton Applied Research, USA).

RSC Advances Accepted Manuscript

View Article Online
DOI: 10.1039/C6RA08774D

Published on 22 June 2016. Downloaded by Sichuan University on 24/06/2016 05:17:58.

In order to compare the changes of phase composition and structure of NMC electrodes under different states, X-ray diffraction (XRD) tests were carried out using Cu-Kα radiation in the range from 10 to 70 º at a scanning rate of 0.04 º s^{-1} on a Philips X'Pert pro MPD machine.

2.3. Measurement of cell strains

The testing cell is a sealed container composed of 304 stainless steel (SS), so resistance strain gauges for metals (Zhonghang Electronic Measuring Instruments Co. Ltd., China) were chosen for measuring the strains and consequently evaluating the stresses in lithium cells under different conditions. The gauge has a size 0.3×1.8 mm and a maximum strain range of 2%. The accuracy and the resistance are about 1 με and 120 Ohm, respectively. The strain gauge consists of a grid of wire filament on an insulated rear side which supports a metallic foil pattern. To allow the strains to be transferred from the test specimen to the foil through the adhesive and strain gauge, the strain gauge needs to be properly mounted onto the shell surface. The cathode shell was firstly polished with sandpaper, and cleaned by ethanol. Glue was pasted on the dried clean surface for adhering the strain gauge. After being well adhered to the cathode shell surface, the gauge was connected to a stress-strain testing system (Donghua testing technology Co. LTD, China). At the same time, the cell was connected to the electrochemical testing system to evaluate the relationship between strains and electrochemical performance of NMC cells under different operating conditions, and the principle diagram and images of the testing systems are shown in Fig. 1.

3. Results and discussion

3.1. Influence of strain gauge installation on the electrochemical performance

In order to evaluate the influence of strain gauge installation on the electrochemical performance of the lithium cells, galvanostatic charge/discharge tests before and after installing strain gauge were

RSC Advances Accepted Manuscript

View Article Online
DOI: 10.1039/C6RA08774D

Published on 22 June 2016. Downloaded by Sichuan University on 24/06/2016 05:17:58.

carried out at 25 ºC, and the typical curves are compared in Fig. 2. After installing the strain gauge, the galvanostatic charge/discharge curves from 2.8 to 4.3 V at 1.0 C current rate are coincidence under the same testing conditions, indicating that the installation of strain gauge has a negligible effect on the electrochemical performance of NMC cells. Therefore, such non-destructive method can reflect the stress changes of lithium ion cells without altering their performance.

3.2. Temperature correction and deformation analysis of the cells

Because the most desirable strain gauge materials are sensitive to temperature variations, resistance wires of the strain gauge will deform when the surrounding temperature is changed, which will result in resistance change and produce test inaccuracies and even errors. Due to the low thermal expansion coefficient [11], the quartz glass was chosen to characterize the test accuracy, and the measured strain data will be calibrated to authentically reflect the safety properties of the battery materials and combined electrolyte system. The strain changes could be caused by the active material decomposition or volume changes of electrolyte, and/or the expansion of the cell case and related accessories. In order to obtain the strain changes from the NMC electrode material, two types of lithium ion cells were assembled under the same conditions, *i.e.* one is a normal cell (abbreviate C) with active material and electrolyte, and the other is a reference cell (abbreviate R) which is same as the normal cell but with no active material. These test specimens were heated to the evaluated temperatures and kept for a period before being naturally cooled down by air. As the temperature increases from 25 to 50 ºC, the strain changes of the normal cell, reference cell, and quartz glass are compared in Fig. 3(a). The strain values of the quartz glass decrease quickly to -580 με in less than 1 h, while that of the reference cell decrease slowly to -120 με in about 2 h. However, the strain value reaches more slowly +100 με in 5 h when NMC electrode is added. Noticeably, the

RSC Advances Accepted Manuscript

View Article Online
DOI: 10.1039/C6RA08774D

Published on 22 June 2016. Downloaded by Sichuan University on 24/06/2016 05:17:58.

strain values of the quartz glass and the reference cell decrease very quickly in a short time before reaching a stable state. However, the strain values of the normal cell increase and reach a constant state much more slowly. The same strain gauges were used and the tests were carried out under the same environmental conditions, so the strain difference is from the substrates. The substrates with larger deformation than that of the resistance wires will cause the negative strain (compression), while the deformation of the substrates lower than that of the resistance wires will cause the positive strain (tension). If the substrates change little, the compression and tension of resistance wires will produce negative strain and positive strain, respectively. The normal cell has the highest deformation, and the deformation of the reference cell is much higher than that of quartz glass. The quartz glass has a negligible deformation at 50 ºC, so the maximum negative strain is from the compression of resistance wires, and the as-obtained strain values reflect the changes of strain gauge itself. As the substrate changes from quartz glass to the SS shell of reference cell, the strain values increase greatly under the same conditions, indicating that the deformation of the SS substrate increase to make the compression of resistance wires weak. The strain values change from negative to positive and reach maximum when NMC electrode is added to the reference cell, indicating that electrode causes the increase of substrate deformation to change the resistance wires from compression to tension. Therefore, the test strain values are the combination from both the strain gauge and test specimens, and the substrate deformation from the swelling of SS shell causes the increase of strain values. As for the cells at open-circuit states, the normal cell has much higher strain values than that of the reference cell under the same conditions, indicating the higher deformations of the normal cell is due to the NMC electrode. The quartz glass reflects the temperature effect of the strain gauge, so all the strain values used for calculating stresses will be corrected by eliminating the temperature effect of the strain gauge.

RSC Advances Accepted Manuscript

View Article Online
DOI: 10.1039/C6RA08774D

Published on 22 June 2016. Downloaded by Sichuan University on 24/06/2016 05:17:58.

158 In order to determine the stresses from the measured strains, the stress-strain relationship of cathode
159 shell needs to be determined. The deformations of the SS cathode shell and quartz glass were
160 further tested within a wide temperature range of 25 ~ 80 ºC. The strain values obtained from the
161 tests during the increasing/decreasing processes of temperature are summarized in Fig. 3(b).
162 Apparently the strain values can be recovered to 0 when the temperature decreases from 80 to 25 ºC,
163 indicating only elastic deformation occurs, thus elastic theory can be used for calculating the
164 stresses using the measured strains, as discussed in the next section.

165

166 ***3.3. Strain-stress relationship of lithium cells***

167 The radius (R) and thickness (t) of the SS cathode shell of the cells are 10 mm and 0.15 mm,
168 respectively. Thus the ratio of t/R is 0.015/10 which is much smaller than 0.1, and the cathode shell
169 can be regarded as a thin-walled plate. As aforementioned the cathode shell of the cells exhibits
170 small elastic deformation during the testing processes. If the distribution of the stresses P_z along the
171 longitudinal direction of the cathode shell is assumed to be uniform, a rigorous relationship between
172 the P_z and the stresses can be found using the elastic theory for shells as follows.

173 The construction of the cell is illustrated in Fig. 4(a), and the cathode shell laminate is cut off by
174 two cylinders and two radial transverse sections to produce a small element, as shown in Fig. 4(a-1)
175 and (a-2). The radius of the two cylinders are r and $r+dr$, respectively. The angle between the
176 two transverse sections is $d\theta$. From Fig. 4(a-3) and (a-4), axial bending moment and transverse
177 shear stress on the two cylinders are M_r, $M_r+\left(dM_r r/dr\right)dr$ and Q_r, $Q_r+\left(\frac{dQr}{dr}\right)_{dr}$, respectively.
178 Circumferential bending moment on the two cylindrical surfaces is both M_θ. External stress on two
179 cylindrical surfaces is P_z.

180 According to the moment equilibrium of the element, algebraic sum of all internal moments and

RSC Advances Accepted Manuscript

View Article Online
DOI: 10.1039/C6RA08774D

external moments on the tangent line of cylinders is 0:

$$\left(M_r+\frac{dM_r}{dr}dr\right)(r+dr)d\theta-M_r r d\theta-2M_\theta dr\sin\frac{d\theta}{2}+Q_r r d\theta dr+P_z r d\theta dr\frac{dr}{2}=0 \quad (1)$$

with $\sin\frac{d\theta}{2}\approx\frac{d\theta}{2}$ when θ is small. Ignoring the second-order terms, this becomes

$$M_r+\frac{dM_r}{dr}r-M_\theta+Q_r r=0 \quad (2)$$

The deformation of mid-plane caused by the uniform pressure is axially symmetrical. Therefore, the deformation, w, only depends on the radius r. As shown in the Fig. 4(b), AB is a line on the radial section whose vertical distance to mid-plane is z. The radius of A and B are r and $r+dr$, respectively, so $AB=dr$. The lines of mn and m_1n_1 pass through the points of A and B, respectively. Both lines are vertical to the mid-plane. When the cathode laminate deforms, A and B move to A_1 and B_1, respectively. Therefore, the strains are

$$\varepsilon_r=\frac{z(\varphi+d\varphi)-z\varphi}{dr}=z\frac{d\varphi}{dr} \quad (3a)$$

$$\varepsilon_\theta=\frac{2\pi(r+z\varphi)-2\pi r}{2\pi r}=z\frac{\varphi}{r} \quad (3b)$$

Under small deformation, $\varphi=-\frac{dw}{dr}$, Equations (3) and (4) are rewritten as

$$\varepsilon_r=-z\times\frac{d^2w}{dr^2} \quad (4a)$$

$$\varepsilon_\theta=-\frac{z}{r}\times\frac{dw}{dr} \quad (4b)$$

By Kirchhoff-love assumption every point in the laminate is under the two-direction stress state when the cathode laminate deforms. According to the generalized Hooke's law, the physical equations of the cathode laminate are:

$$\sigma_r=\frac{E}{1-\mu^2}(\varepsilon_r+\mu\varepsilon_\theta) \quad (5a)$$

$$\sigma_\theta=\frac{E}{1-\mu^2}(\varepsilon_\theta+\mu\varepsilon_r) \quad (5b)$$

Published on 22 June 2016. Downloaded by Sichuan University on 24/06/2016 05:17:58.

RSC Advances Accepted Manuscript

View Article Online
DOI: 10.1039/C6RA08774D

Published on 22 June 2016. Downloaded by Sichuan University on 24/06/2016 05:17:58.

Combining above equations and substituting (4) into (5), the stresses can be written as:

$$\sigma_\theta = -\frac{Ez}{1-\mu^2}\left(\frac{1}{r}\frac{dw}{dr} + \mu\frac{d^2w}{dr^2}\right) \tag{6a}$$

$$\sigma_r = -\frac{Ez}{1-\mu^2}\left(\frac{\mu}{r}\frac{dw}{dr} + \frac{d^2w}{dr^2}\right) \tag{6b}$$

After integration, the bending moment can be obtained:

$$M_r = \int_{\frac{-t}{2}}^{\frac{t}{2}} \sigma_r z dz = -D\left(\frac{d^2w}{dr^2} + \frac{\mu}{r}\frac{dw}{dr}\right) \tag{7a}$$

$$M_\theta = \int_{\frac{-t}{2}}^{\frac{t}{2}} \sigma_\theta z dz = -D\left(\mu\frac{d^2w}{dr^2} + \frac{1}{r}\frac{dw}{dr}\right) \tag{7b}$$

where $D = \frac{Et^3}{12(1-\mu^2)}$).

Substituting (7(a)(b)) into (1) and with some arrangements, the following equation can be obtained.

$$\frac{d}{dr}\left[\frac{1}{r}\frac{d}{dr}\left(r\frac{dw}{dr}\right)\right] = \frac{Q_r}{D} \tag{8}$$

The distribution of the transverse load is assumed to be uniform. As shown in the Fig. 4(c), the shearing force on the cross section of the cylinder whose radius is *r* is as follows:

$$Q_r = \frac{\pi r^2 p}{2\pi r} = \frac{pr}{2} \tag{9}$$

Substituting (9) into (8) we have

$$\frac{d}{dr}\left[\frac{1}{r}\frac{d}{dr}\left(r\frac{dw}{dr}\right)\right] = \frac{pr}{2D} \tag{10}$$

After integrations, the bending deformation of the mid-plane is:

$$w = \frac{pr^4}{64D} + \frac{C_1 r^2}{4} + C_2 \ln r + C_3 \tag{11}$$

where, C_1, C_2, C_3 are the constants to be determined. Since the deformation and slope of the laminate are limited values, C_2=0. The rim of the cathode laminate is assumed to be clamped, so

RSC Advances Accepted Manuscript

View Article Online
DOI: 10.1039/C6RA08774D

Published on 22 June 2016. Downloaded by Sichuan University on 24/06/2016 05:17:58.

r=R, $\frac{dw}{dr}=0$, and $w=0$

Finally the deformation is calculated as:

$$w=\frac{p}{64D}(R^2-r^2)^2 \quad (12)$$

Substituting (12) into (11) gives:

$$M_r=\frac{p}{16}[R^2(1+\mu)-r^2(3+\mu)] \quad (13a)$$

$$M_\theta=\frac{p}{16}[R^2(1+\mu)-r^2(1+3\mu)] \quad (13b)$$

So the stresses are:

$$\sigma_r=\frac{M_r}{t^2/6}=\frac{3}{8}\frac{p}{t^2}[R^2(1+\mu)-r^2(3+\mu)] \quad (14a)$$

$$\sigma_\theta=\frac{M_\theta}{t^2/6}=\frac{3}{8}\frac{p}{t^2}[R^2(1+\mu)-r^2(1+3\mu)] \quad (14b)$$

The stresses at the centre of the cathode laminate (*i.e.* r=0) are found to be:

$$\sigma_r=\sigma_\theta=\frac{E}{1-\mu}\varepsilon_\theta \quad (15)$$

The material of the cell shell is 304 stainless steel which has a Young's modulus E of =193 GPa and a Poisson's ratio μ of 0.28 at 25 ºC [12]. Therefore, the stress at the centre of the cell shell can be calculated using the measured strain according to Eq. 15. From Eq. 14(a)(b), the maximum stress is at the centre of the cell plate, and the stress distribution along the radius across the whole surface of the cell is supplied in Fig. 4(d), which is of most interest for evaluating the safety issues of the cell. The normalized stress and normalized radius are obtained by dividing the maximum stress and maximum radius, respectively. The stresses along the axial direction and radial direction decrease differently with the increase of radius, which is significant to analyse the stress distribution and the possible failure position of the cell surface.

3.4. Influence of ambient temperature on the stresses in cells

RSC Advances Accepted Manuscript

View Article Online
DOI: 10.1039/C6RA08774D

Published on 22 June 2016. Downloaded by Sichuan University on 24/06/2016 05:17:58.

Since both the strain gauge and the specimen are sensitive to ambient temperature, the strain gauges are designed to minimize the sensitivity to temperature by compensating the thermal expansion of the specimen materials. In order to eliminate the influence of electrochemical activation on the stresses, the cells were galvanostatically charged/discharged for 10 cycles and discharged to 2.8 V to reach a stable state. The cycled and stable cells were kept for over 20 h in an oven with various temperatures to evaluate the effects of ambient temperature on the stresses of the electrode. Under a series of ambient temperature (i.e. 25, 50, 60, 70, 80 ºC) the stress changes of the normal cells and the reference cells at the same charge states were monitored, and the testing results are shown in Fig. 5. The stable stress values of the normal cell C and the reference cell R are almost zero and have no change at 25 °C. However, the values of C and R respectively increase gradually to 125 MPa and 95 MPa when the ambient temperature reaches 50 °C. The values of C and R respectively increase quickly to 126 MPa and 113 MPa when the temperature further increases to 60 °C. The values of C and R respectively increase to 175 MPa and 162 MPa when the temperature further increases to 70 °C. As the temperature further increases to 80 °C, the stress values of the normal cell C increase quickly and continuously above 200 MPa, and have a jump above 240 MPa when the heating period is 18 h, while that of the reference cell R have an abrupt increase and reach a stable value of 170 MPa gradually. Under the same conditions, the stresses of the normal cells are always higher than that of the reference cells, and higher temperature results in higher stress values. Comparing the stress values of the cells under the same conditions, the higher stress values of the normal cells are from the NMC electrode.

No obvious signal for Mn, Ni, and Co is detected in the electrolyte when the charged $Li_{1.1}(Mn_{1/3}Ni_{1/3}Co_{1/3})_{0.9}O_2$ cell is stored in a 55 °C oven for 3 weeks [6], and the amounts of Ni, Co, and Mn dissolved in the electrolyte are respectively 48.0, 50.5, and 42.4 ppm when

RSC Advances Accepted Manuscript

View Article Online
DOI: 10.1039/C6RA08774D

Published on 22 June 2016. Downloaded by Sichuan University on 24/06/2016 05:17:58.

$Li[Mn_{1/3}Ni_{1/3}Co_{1/3}]O_2$ electrode is immersed in the electrolyte at 55 °C for 10 days [13]. Correlating this information with the stress changes of the normal cells and reference cells, the stress is mainly caused by the thermal expansion of cell case in the temperature range of 50 ~ 60 °C, and the extra stress values of the normal cells are contributed from the volume expansion of the NMC electrode, including active material, conductive additive and binder. Though the stable stress values of the normal cell at 60 °C is close to that at 50 °C, the stress values at 60 °C increases much faster than that at 50 °C, indicating that the volume expansion of the NMC electrode reaches a maximum state at different rates within the temperature range and a higher temperature enhances the increasing rate of the stress. The stress values of the reference cells at 70 °C are similar to that at 80 °C, indicating the thermal stress of the SS cell case reach a maximum state when the temperature is 70 °C, and quickly becomes stable when the temperature is 80 °C. $LiPF_6$ can be resolved into PF_5 at 70 °C, and PF_5 will react with the solvents of EC and DMC at 85 °C [14]. Therefore, the extra increment of the stress values of the normal cells is mainly from the decomposition of $LiPF_6$ when the temperature increases to 70 °C, and the much more increment is mainly from the reaction of the decomposition product of PF_5 with the solvents in the electrolyte at 80 °C. The produced gases in the normal cells will produce continuously increasing stress with the prolonging of the heating time at 80 °C.

3.5. Stress changes during cycles

In order to investigate the stress changes during galvanostatic charge/discharge cycles at low current density, the stresses of the fresh cells were real-time monitored at 25 ºC. The stress curves corresponding to the charge/discharge curves at 0.5 C rate between 2.8 V and 4.3 V are shown in Fig. 6. During the charge process of NMC material, lithium ions are continually extracted from the structure and the decrease of lithium ions result in the increase of the reduced ions of Ni, Co and

RSC Advances Accepted Manuscript

View Article Online
DOI: 10.1039/C6RA08774D

Mn in oxidation state to keep charge balance, so the lattice constants of *a* and *c* change in the α-$NaFeO_2$ layered crystal structure. The *a* decreases whilst the *c* increases due to an increasing electrostatic repulsion [15]. These changes of the parameters of *a* and *c* produce microscale stress between particles, which further develop to the macroscale stress monitored by the strain gauge. From the curves, such stress increases at different rates during a charge/discharge cycle. At the beginning of the charge process, the potential increases quickly from 2.8 V to 3.6 V, while the corresponding stress increases gradually from 0.0 to 0.3 MPa. At the potential platform from 3.6 to 3.8 V, the stress value increases from 0.3 MPa to 4.6 MPa, indicating lithium ions extraction causes the change in lattice volume of the crystal in the single phase region of electrode material [16], which results in the increase of stress. When the potential is increased from 3.8 V to 4.3 V, the stress increases quickly to the maximum value of 9.2 MPa at the highest potential, along with the large volume changes from the high electrostatic repulsion. Therefore, the stress value of the cell is closely related to the charge state of the cells, which has also been reported in [17]. The stress increases with the potential within the testing window, and both stress and potential reach maximum values simultaneously at the end of charge process, indicating the increased stress is caused by the volume changes of the NMC electrode into which lithium ions are inserted. During the discharge process, the stress decreases differently with the decrease of potential. During initially discharge, from 4.3 V to 3.8V, the stress decreases rapidly to 3.9 MPa, followed by a gradual relaxation as more lithium ions are inserted. At the discharge platform from 3.8 V to 3.6 V, the stress value decreases from 3.9 MPa to 1.1 MPa. However, the stress value is 0.5 MPa, not initial 0, when the potential restore to 2.8 V, indicating there is a residual stress during the charge/discharge cycle, which is similar to the irreversible increase in stack stress to permanent volumetric expansion of graphite anode [18]. Such residual stress will accumulate and lead to the unrecoverable deformation of

Published on 22 June 2016. Downloaded by Sichuan University on 24/06/2016 05:17:58.
RSC Advances Accepted Manuscript

View Article Online
DOI: 10.1039/C6RA08774D

Published on 22 June 2016. Downloaded by Sichuan University on 24/06/2016 05:17:58.

the cell during cycles, which could evolve into safety problems like swelling or bulging.

In order to investigate the relationship between the capacity fade and residual stress at high current density, the normalized capacities and corresponding residual stress values of the cell during 100 cycles between 2.8 V and 4.3 V at 1 C rate are summarized in Fig. 6 (c). After 100 cycles, the residual stress accumulates from 0 to 37.8 MPa, and the capacity declines to 88.7 % of the initial capacity. During the continuous charge/discharge cycles, the capacity fades gradually but the residual stress increases quickly, as a result of the deformation from the loss of cycled lithium ions, similar to that in graphite [1].

CV tests are carried out on the cells which are discharged to 2.8 V after different cycles to better understand the increased residual stress and decreased capacity, and the results are shown in Fig. 6(d). The oxidization potential (E_O), reduction potential (E_R), potential difference between oxidization peak and reduction peak (ΔE), oxidation peak current (I_O) and reduction peak current (I_R) are listed in Table 1. The 2nd and 3rd CV curves are almost coincident except the higher oxidization peak intensity of the 2nd curve and the lower oxidization peak potential of the 3rd curve, indicating the higher reaction activity of the 2nd cycle and the lower polarization degree of the 3rd cycle. The oxidization peak at around 3.87 V and the reduction peak at around 3.68 V are associated to the de-intercalation and intercalation of lithium ions inside the host matrix, respectively. The Ni^{2+}/Ni^{4+} accounts for the oxidation peak at 3.87 V [19] and the reduction peak at 3.67 V [20]. However, the redox peak intensities decrease greatly after 100 cycles and the potential difference between oxidization peak and reduction peak increases overwhelmingly, suggesting the reaction activity decreases and the reaction resistance increases during cycling process, which results in the decrease of capacity and the increase of residual stress.

RSC Advances Accepted Manuscript

View Article Online
DOI: 10.1039/C6RA08774D

Published on 22 June 2016. Downloaded by Sichuan University on 24/06/2016 05:17:58.

3.6. Stress and structure changes during overcharge and over-discharge processes

From above analysis, charge state is found to greatly affect the stress values. In order to investigate the stress changes of the cells under some extreme conditions like overcharge (abbreviate OC) and over-discharge (abbreviate OD), the stress changes were monitored when they are respectively charged to 5 V and discharged to 0 V at 1.0 C rate at 25 ºC, and the results are summarized in Fig. 7. As shown in Fig. 7 (a), the stress increases slowly and almost linearly from 0 to 9.9 MPa with a low slope of 7.6 MPa/h when the potential of the cell increases from 2.8 V to 4.3 V, close to that in the normal potential window shown in Fig. 6. So, the battery is under a normal state in this charge process. However, the stress increases abruptly from 10.0 MPa to 55.5 MPa when the potential increases from 4.7 V to 5.0 V, and the slope jumps to 225.5 MPa/h. The cell above 4.7 V is regarded as in an overcharge state [21], so the stress increases rapidly in the overcharge state, which is attributed to the decomposed gases from the electrolyte [15].

During the over-discharge process from 4.3 V to 2.8 V, the stress drops slowly from 10.0 MPa to 0.2 MPa in an almost liner way, as shown in Fig. 7(b), similar to above results. However, the stress decreases linearly to -1.5 MPa when the potential decreases to 1.2 V. Furthermore, the decreasing slope of the stress keeps constant when the potential drops from 4.3 V to 1.2 V. The cyclability of the cell affects little by over-discharge to 2.0 V or 1.5 V, and the capacity loss is close to that of the similar cell cycled between 3.0 and 4.2 V [22]. Below 1.2 V, the potential decreases slowly and exhibits a quasi-plateau till 0.6 V, where the corresponding stress decreases in a stair step till -5.0 MPa. Below 0.6 V, the potential decreases quickly to 0.0 V, but the stress increases abnormally in a linear way to -1.8 MPa. The stress values change from positive to negative during the over-discharge process, indicating the stress changes from tension to compression, which is from the negative deformation of the surface shell. With the decrease of the cut-off potential, lithium ions

RSC Advances Accepted Manuscript

View Article Online
DOI: 10.1039/C6RA08774D

Published on 22 June 2016. Downloaded by Sichuan University on 24/06/2016 05:17:58.

continuously intercalate the electrode material to destroy the crystals [23,24], which results in the decrease of volume and the increase of the negative stress values when the potential decreases from 1.2 V to 0.6 V. Over-discharge to 1.0 and 0.5 V leads to cell's capacity loss of 29 and 38 %, respectively, which is significantly higher than normally cycled cells [22]. Large amount of CO_2 and hydrocarbons as well as CO have been found in the over-discharged cell [25], and electrolyte decomposition is accelerated in the over-discharged state [26]. The decomposition of the electrolyte is dependent on the changes of surface conditions at the cathode. Therefore, with the continuous increase of inserted lithium ions, the crystal structure of the NMC material starts to breakdown to reduce deformation when the potential drops to 1.2 V, so the discharge process becomes difficult and the corresponding stress exhibits negative values. The completed destruction results in the lowest negative stress when the potential is 0.6 V. The produced gases or hydrocarbon will increase anomaly the stress below 0.6 V, as shown in the curve. Though the potential decreases slowly below 1.2 V, the stress has several plateaus during the decreasing process. The plateaus may correspond to the damage process of the crystals. The possible mechanisms are further confirmed by the following XRD and EIS tests.

In order to detect the composition and the microstructure of the active materials under different charge states, the NMC electrodes were analysed by XRD technique, and the patterns are supplied in Fig. 7. Considering the low loading density of active material, the aluminium current collector of the NMC electrode was not removed for XRD characterization. In these patterns, all the index peaks except the obvious Al peak at around 65 º are attributed to the samples at different charge states. Noticeably, the XRD patterns of the pristine and the overcharged samples are almost identical and the average crystallite size of the pristine and the overcharged is 46.265 and 52.765nm, respectively, indicating the crystal structure changes during the overcharge process. All peaks of

RSC Advances Accepted Manuscript

View Article Online
DOI: 10.1039/C6RA08774D

Published on 22 June 2016. Downloaded by Sichuan University on 24/06/2016 05:17:58.

both samples match well with that of the hexagonal α-$NaFeO_2$ structure with the R3m space group, indicating the existence of layered structure [27-29]. After overcharge, lithium ions are extracted from the NMC, the peak densities of the (101), (102) and (104) decline, and the lattice constants of the *a* and *c* of the NMC change from 2.860 and 14.225 Å to 2.831 and 14.322 Å, respectively. Furthermore, the high potential will lead to the decomposition of electrolyte. These changes cause the increase of stress during overcharge process, in consistent with above stress analysis results. However, the main characteristic peaks of the NMC disappear in the over-discharged pattern, and more amorphous characteristics appear except the peak at around 38 º, suggesting the crystal structure of the over-discharged sample destroys, which also confirms with above stress changes. The amorphous products are probably the X-ray undetectable nano-sized mixtures, similar to that in the over-discharged $LiFePO_4$, $LiNiO_2$, and $LiMn_2O_4$ [24] such products result in the decrease of volume and electrostatic repulsion to produce negative deformation of shell to produce negative stress, agreeing well with above results.

In order to compare the interface behaviour of the electrodes under different charge states, the cells were further analysed with EIS technique, and the curves are supplied in Fig. 7(d). The fresh cells were galvanostatically charged or discharged to the referred potential for the EIS tests. Except that of the over-discharged curve, all the curves at other charge states have two semicircles in the high-to-medium frequency region, indicating a similar electrode reaction process. The zoomed-in section in Fig. 7(e) clearly shows the constitutions of the semicircles. In the curves of 2.8 V and 4.3 V, the two semicircles grow with the increase of charge voltage limit, similar to Zheng's report [27]. The semicircle in the medium-to-low frequency region becomes big abnormally when the cell is overcharged. The intercept of the curves on the Z' real axis in the high frequency region is attributed to the ohmic resistance of the electrolyte solution (R_s). The semicircle in the high-to-medium

RSC Advances Accepted Manuscript

View Article Online
DOI: 10.1039/C6RA08774D

Published on 22 June 2016. Downloaded by Sichuan University on 24/06/2016 05:17:58.

frequency region corresponds to the impedance of the solution film resistance (R_f) on the electrode surface. The semicircle in the medium-to-low frequency region is related to the solid electrolyte interface (R_{SEI}) and charge transfer resistance (R_{ct}). The oblique line in the low frequency region is concerned to Warburg impedance W which concerns the semi-infinite diffusion of lithium ions in the bulk electrode. Using ZsimpWin and Z-view softwares with the R(QR)(QR)(QR)W model supplied in Fig. 7(f), the EIS curves are fitted well, indicating lithium ions diffuse in the crystal structure after reacting with electrode materials. Due to the non-homogeneity such as porosity, roughness, and geometry in the system, constant phase element (CPE) Q is substituted for traditional capacitance C in the model. In the equivalent circuit, the Q_f, Q_{SEI} and Q_d correspond to the constant phase elements of the electrolyte film, SEI film and film/electrode interface, respectively [30]. During the charge process, lithium ions are extracted from the NMC material to form $Ni_{1/3}Co_{1/3}Mn_{1/3}O_2$ with high metal valences, so the charge transfer reaction becomes difficult and the high metal valences accelerates the oxidization of the electrolyte to produce gases to form a thick film on the electrode surface. All these result in the big semicircles, agreeing with the testing results. According to the simulation results supplied in Table 2, the Ohmic resistances of liquid charge-transfer resistance of the 2.8 V and 4.3 V are close, but that of the over-discharged and overcharged increase greatly, indicating the conductivity of the electrolyte near the electrode surface changes, which is from the changed composition after over-discharge or overcharge. The large differences of film resistance and charge transfer reaction resistance show that the electrode surface changes greatly under different charge states, which may be from the different compositions or structure of the NMC electrode material. All these changes cause the stress change in the cell shell to produce possible safety issues.

In order to detect the stress from lithium anode, the strain gauge was adhered to anode shell, and the

RSC Advances Accepted Manuscript

View Article Online
DOI: 10.1039/C6RA08774D

Published on 22 June 2016. Downloaded by Sichuan University on 24/06/2016 05:17:58.

stresses were real-time monitored under the same testing conditions with NMC cathode. From the testing results in Figure S1, the stress values are close to the minimum detection limit of the strain gauge, indicating the stress change of the lithium anode shell is too low to be detected by the strain gauge with a detection limit of 1 με. Lithium ions are extracted from NMC cathode to deposit on the lithium surface which is in the electrolyte during charge process, while lithium ions are extracted from lithium anode to insert NMC cathode during discharge process. As for lithium anode, lithium ions are excessive in the test cells, and lithium ions extraction/deposition reactions take place at the lithium surface wetted by the electrolyte, instead of the crystal lattice like that in NMC cathode to cause volume changes. Furthermore, lithium is a soft metal which can resist the strain during electrode reaction processes, and the flexible polymer separator along with electrolyte can buffer the large volume change of NMC cathode. Therefore, the stress change from the lithium anode is low enough to be neglected, and the strain of the NMC shell is mainly from the lithium ions processes of NMC electrode in the test cells.

3.7. Relationship between charge states and stress changes

According to above analysis, the relationship between charge states and stress changes at 25 °C is constructed in Fig. 8. The stress continuously increases from -5.0 MPa to 55.5 MPa when the state-of-charge (SOC) changes from over-discharge OD to overcharge OC, but the cell exhibits good electrochemical performance in the normal region with SOC increasing from 0 to 100%. Beyond the normal region, the electrochemical performance becomes poor, and the stress increases differently. As the potential discharges to 2.8 V, the residual stress value reaches 0.2~0.5 MPa when the current rate is 1C. As mentioned before, the residual stress accumulates to 37.8 MPa after 100 cycles, and the polarization become high and the capacity fades to 88.7 %, so the increased residual

RSC Advances Accepted Manuscript

View Article Online
DOI: 10.1039/C6RA08774D

Published on 22 June 2016. Downloaded by Sichuan University on 24/06/2016 05:17:58.

stress undermines the electrochemical performance. The stress value ranges from 9.9 MPa to 55.5 MPa during overcharge process from 4.3 V to 5.0 V, while that from 0.2 MPa to -5.0 MPa during the over-discharge process from 2.8 V to 0.0 V. Under the over-discharge state, the stress of the cell first decreases and then increases because of the different reaction process. Therefore, the emergence of high pressure on the surface of the cell case means the degradation of the electrochemical performance, which is significant for the safety management of batteries in applications.

4. Conclusions

A non-destructive method has been developed to real-time monitor the surface stress changes of a SS cell case for the safety management. The temperature sensitivity and stress properties of the strain gauges have been investigated, and temperature correction has been conducted. The stress-strain relationship of the cell case has been established according to the derived stress calculation formula. The stress values of the NMC cells under different states have been discussed. As the cells are open circuit, the surface stress mainly originates from the thermal stress of case at temperatures from 50 to 70 ºC, but the continuously increasing stress at 80 ºC is due to electrolyte decomposition in addition to the volume expansion of electrode and thermal stress of case. The surface stress is greatly affected by charge state, and the stress value increases from 0.0 to the maximum value of 9.2 MPa when potential increases from 2.8 to 4.3 V at 0.5 C current rate, but the stress does not restore to 0.0 MPa when potential decreases to 2.8 V. The accumulated residue stress is 37.8 MPa, while the capacity degradation is 11.3 % compared to the initial capacity after 100 cycles at 1.0 C current rate. During the overcharge to 5.0 V, the stress increases slowly to 10.0 MPa at 4.7 V, and then increases quickly to 55.5 MPa. During the over-discharge to 0.0 V, the stress

RSC Advances Accepted Manuscript

View Article Online
DOI: 10.1039/C6RA08774D

Published on 22 June 2016. Downloaded by Sichuan University on 24/06/2016 05:17:58.

value decreases linearly from 10 to -2.0 MPa when potential decreases from 4.3 to 1.2 V, and then decreases to -5.0 MPa from 1.2 to 0.6 V, while increases abnormally to -1.8 MPa from 0.6 to 0.0 V. Various techniques have been used to analyse the electrode reaction processes. The increased surface stress worsens the electrochemical performance, and their relationship has been analysed. The relationship between stress and potential can potentially serve as a useful tool to monitor the electrochemical performance and failure of batteries.

The surface stress changes can be monitored successfully by strain gauges in lithium cells. A sealed battery can be regarded as a pressure vessel where electrode reaction takes place, and the inner pressure would cause the deformation of the shell to produce stress, so strain gauge could be used to monitor the strain-stress of a full battery, and some pictures of the stress testing system for a practical full battery are supplied in Figure S2. The stress measurements can be further combined with computer simulation calculations on the surface for cross validations and to predict the stress changes in the complex processes involving chemical reaction and thermal effects. Compared the surface stress to the stress threshold value of the battery package, special techniques (including ending, blocking, cutting, or injecting chemicals, *etc*.) could be utilized to eliminate safety issues. Therefore, this initial work demonstrates the possibility to monitor the surface stress changes of cells using strain gauges as an effective and economical way which may greatly improve the safety management of batteries.

Acknowledgments

We gratefully acknowledge the financial support from the National Science Foundation of China (Grant No. 21206099 and 21576170), and the Experimental Technical Project (2015-0141) of Sichuan University.

RSC Advances Accepted Manuscript

View Article Online
DOI: 10.1039/C6RA08774D

Published on 22 June 2016. Downloaded by Sichuan University on 24/06/2016 05:17:58.

References

1. Cannarella J, Arnold CB. Stress evolution and capacity fade in constrained lithium-ion pouch cells. *Journal of Power Sources.* 2014;245(1):745-751.
2. Çapraz ÖÖ, Shrotriya P, Skeldon P, Thompson GE, Hebert KR. Role of oxide stress in the initial growth of self-organized porous aluminum oxide. *Electrochimica Acta.* 2015;167:404-411.
3. Fadda S, Cincotti A, Cao G. The effect of cell size distribution during the cooling stage of cryopreservation without CPA. *AICHE Journal.* 2009;56(8):2173-2185.
4. He YJ, Shen JN, Shen JF, Ma ZF. State of health estimation of lithium-ion batteries: a multiscale gaussian process regression modeling approach. *Aiche Journal.* 2015;61(5):1589–1600.
5. Spotnitz R, Franklin J. Abuse behavior of high-power lithium-ion cells. *Journal of Power Sources.* 2003;113(1):81-100.
6. Amine K. Mechanism of capacity fade of MCMB/$Li_{1.1}(Ni_{1/3}Mn_{1/3}Co_{1/3})_{0.9}O_2$ cell at elevated temperature and additives to improve its cycle life. *Journal of Materials Chemistry.* 2011;21(44):17754-17759.
7. Nam KW, Yoon WS, Yang XQ. Structural changes and thermal stability of charged $Li(Ni_{1/3}Co_{1/3}Mn_{1/3})O_2$ cathode material for Li-ion batteries studied by time-resolved XRD. *Journal of Power Sources.* 2009;189(1):515-518.
8. Wu K, Yang J, Liu Y, et al. Investigation on gas generation of $Li_4Ti_5O_{12}$/$Li(Ni_{1/3}Co_{1/3}Mn_{1/3})O_2$ cells at elevated temperature. *Journal of Power Sources.* 2013;237(3):285-290.
9. Hong CY, Yuan TZ, Bing HY, Qiang L. Research of explosion mechanism of Lithium-ion battery. *Electrochemistry.* 2006;18(6):823-831.
10. Larsson F, Mellander BE. Abuse by external heating, overcharge and short circuiting of commercial Lithium-ion battery cells. *Journal of the Electrochemical Society.* 2014;161(10):A1611-A1617.
11. Sorrell CA, Anderson HU, Ackermann RJ. Thermal expansion and the high–low transformation in quartz. II. Dilatometric studies. *Journal of Applied Crystallography.* 1974;7(5):468-473.
12. Kim H, Kang JY, Son D, et al. Microstructures and mechanical properties of cold-work tool steels: a comparison of 8%Cr Steel with STD11. *CRC Press.* 2014;27(5):242-252.
13. Jang SB, Kang SH, Amine K, Bae YC, Sun YK. Synthesis and improved electrochemical performance of Al $(OH)_3$-coated $Li(Ni_{1/3}Co_{1/3}Mn_{1/3})O_2$ cathode materials at elevated temperature. *Electrochimica Acta.* 2005;50(20):4168–4173.
14. Sloop SE, Kerr JB, Kinoshita K. The role of Li-ion battery electrolyte reactivity in performance decline and self-discharge. *Journal of Power Sources.* 2003;119–121(03):330-337.
15. Lin CK, Ren Y, Amine K, Qin Y, Chen Z. In situ high-energy X-ray diffraction to study overcharge abuse of 18650-size lithium-ion battery. *Journal of Power Sources.* 2013;230(15):32-37.
16. Renganathan S, Sikha G, Santhanagopalan S, White RE. Theoretical analysis of stresses in a lithium ion cell. *Journal of the electrochemical society*. 2010;2(2):156-156.
17. Sethuraman VA, Winkle NV, Abraham DP, Bower AF, Guduru PR. Real-time stress measurements in lithium-ion battery negative-electrodes. *Journal of Power Sources.* 2012;206(1):334–342.
18. Cannarella J, Arnold CB. State of health and charge measurements in lithium-ion batteries using mechanical stress. *Journal of Power Sources.* 2014;269(2):7-14.
19. Idemoto Y, Matsui T. Thermodynamic stability, crystal structure, and cathodic performance of $Li_x(Ni_{1/3}Co_{1/3}Mn_{1/3})O_2$ depend on the synthetic process and Li content. *Solid State Ionics.* 2008;179(17):625-635.
20. Yang S, Wang X, Chen Q, Yang X, Li J, Wei Q. Effects of complexants on $(Ni_{1/3}Co_{1/3}Mn_{1/3})CO_3$ morphology and electrochemical performance of $Li(Ni_{1/3}Co_{1/3}Mn_{1/3})O_2$. *Journal of Solid State Electrochemistry.* 2012;16(2):481-490.

RSC Advances Accepted Manuscript

View Article Online
DOI: 10.1039/C6RA08774D

21. Belov D, Yang MH. Failure mechanism of Li-ion battery at overcharge conditions. *Journal of Solid State Electrochemistry.* 2008;12(7):885-894.

22. Maleki H, Howard JN. Effects of overdischarge on performance and thermal stability of a Li-ion cell. *Journal of Power Sources.* 2006;160(2):1395-1402.

23. Shu J, Shui M, Huang F, et al. A new look at lithium cobalt oxide in a broad voltage range for Lithium-ion Batteries. *The Journal of Physical Chemistry C*. 2010;114(7):3323-3328.

24. Shu J, Shui M, Xu D, Wang D, Ren Y, Gao S. A comparative study of overdischarge behaviors of cathode materials for lithium-ion batteries. *Journal of Solid State Electrochemistry.* 2012;16(2):819-824.

25. Yoshida H, Fukunaga T, Hazama T, Terasaki M, Mizutani M, Yamachi M. Degradation mechanism of alkyl carbonate solvents used in lithium-ion cells during initial charging. *Journal of Power Sources.* 1997;68(2):311-315.

26. Kumai K, Miyashiro H, Kobayashi Y, Takei K, Ishikawa R. Gas generation mechanism due to electrolyte decomposition in commercial lithium-ion cell. *Journal of Power Sources.* 1999;81–82(9):715-719.

27. Zheng H, Sun Q, Gao L, Song X, Battaglia VS. Correlation between dissolution behavior and electrochemical cycling performance for $Li(Ni_{1/3}Co_{1/3}Mn_{1/3})O_2$-based cells. *Journal of Power Sources.* 2012;207(6):134-140.

28. Shaju KM, Rao GVS, Chowdari BVR. X-ray photoelectron spectroscopy and electrochemical behaviour of 4 V cathode, $Li(Ni_{1/2}Mn_{1/2})O_2$. *Electrochimica Acta.* 2003;48(11):1505-1514.

29. Kang CS, Son JT. Synthesis and electrochemical properties of $Li(Ni_{1/3}Co_{1/3}Mn_{1/3})O_2$ cathode materials by electrospinning process. *Journal of Electroceramics.* 2012;29(4):235-239.

30. Kang H, Wang G, Guo H, Chen M, Luo C, Yan K. Facile synthesis and electrochemical performance of LiFePO4/C composites using Fe–P waste slag. *Industrial and Engineering Chemistry Research.* 2012;51(23):7923-7931.

Published on 22 June 2016. Downloaded by Sichuan University on 24/06/2016 05:17:58.

RSC Advances Accepted Manuscript

View Article Online
DOI: 10.1039/C6RA08774D

Tables

Table 1. Values of E_O, E_R, ΔE, I_O and I_R of $Li(Ni_{1/3}Co_{1/3}Mn_{1/3})O_2$ after different cycles.

Cycle	E_O (V)	E_R (V)	ΔE (V)	$I_O \times 10^{-4}$ (A)	$I_R \times 10^{-4}$ (A)
2^{nd}	3.87	3.67	0.20	12.83	-6.16
3^{rd}	3.84	3.67	0.17	11.93	-6.28
100^{th}	3.87	3.53	0.34	3.23	-1.80

Published on 22 June 2016. Downloaded by Sichuan University on 24/06/2016 05:17:58.

RSC Advances Accepted Manuscript

View Article Online
DOI: 10.1039/C6RA08774D

574

575

576 **Table 2 Values of R_s, R_f, R_{SEI}, R_{ct} and W.**

State of charge	R_s(ohm/cm^2)	R_f(ohm/cm^2)	R_{SEI}(ohm/cm^2)	R_{ct}(ohm/cm^2)	$W\times10^{-3}$(ohm/cm^2)
0.0V	9.82	108.07	4.75	1145.61	$1.60*10^9$
2.8V	3.83	13.33	15.55	224.56	11.52
4.3V	3.89	12.33	63.60	128.95	6.53
5.0V	4.50	222.89	2310.53	988.60	1.53

577

Published on 22 June 2016. Downloaded by Sichuan University on 24/06/2016 05:17:58.

RSC Advances Accepted Manuscript

View Article Online
DOI: 10.1039/C6RA08774D

Published on 22 June 2016. Downloaded by Sichuan University on 24/06/2016 05:17:58.

Figure Captions

Figure 1. Images of the NMC coin cell adhered with strain gauges and the corresponding testing platform.

Figure 2. Comparisons of the charge/discharge curves of NMC before/after installing gauges.

Figure 3. (a) Strain curves of the NMC cell, reference cell and quartz glass at 50 °C, and (b) strain curve of the cell shell and quartz glass from 25 to 80 °C.

Figure 4. (a) Schematic diagrams of the stress distribution (a-1), (a-2) and internal forces (a-3), (a-4) of the cell, and (b) deformation analysis when the cathode laminate bends; (c) shearing force of the laminate under uniformly distributed loading; (d) normalized stress distribution along radius.

Figure 5. Stress changes of the NMC cell and reference cell at different ambient temperatures.

Figure 6. (a) Typical galvanostatic charge/discharge curves, and (b) the corresponding stress changes at 0.5 C current rate; (c) the residual stress during cycles at 1.0 C current rate; (d) different CV curves of the NMC cell at a scanning rate of 0.2 mV s^{-1}.

Figure 7. The stress changes of the NMC cell during (a) overcharge process, and (b) overdischarge process; (c) XRD patterns of the NMC material, and (d) EIS curves of the NMC cell at different charge states; (e) part amplified, and (f) the corresponding fitting model of the EIS curves.

Figure 8. The relationships between stress changes, state of charge and electrochemical performance at room temperature.

RSC Advances Accepted Manuscript

View Article Online
DOI: 10.1039/C6RA08774D

Published on 22 June 2016. Downloaded by Sichuan University on 24/06/2016 05:17:58.

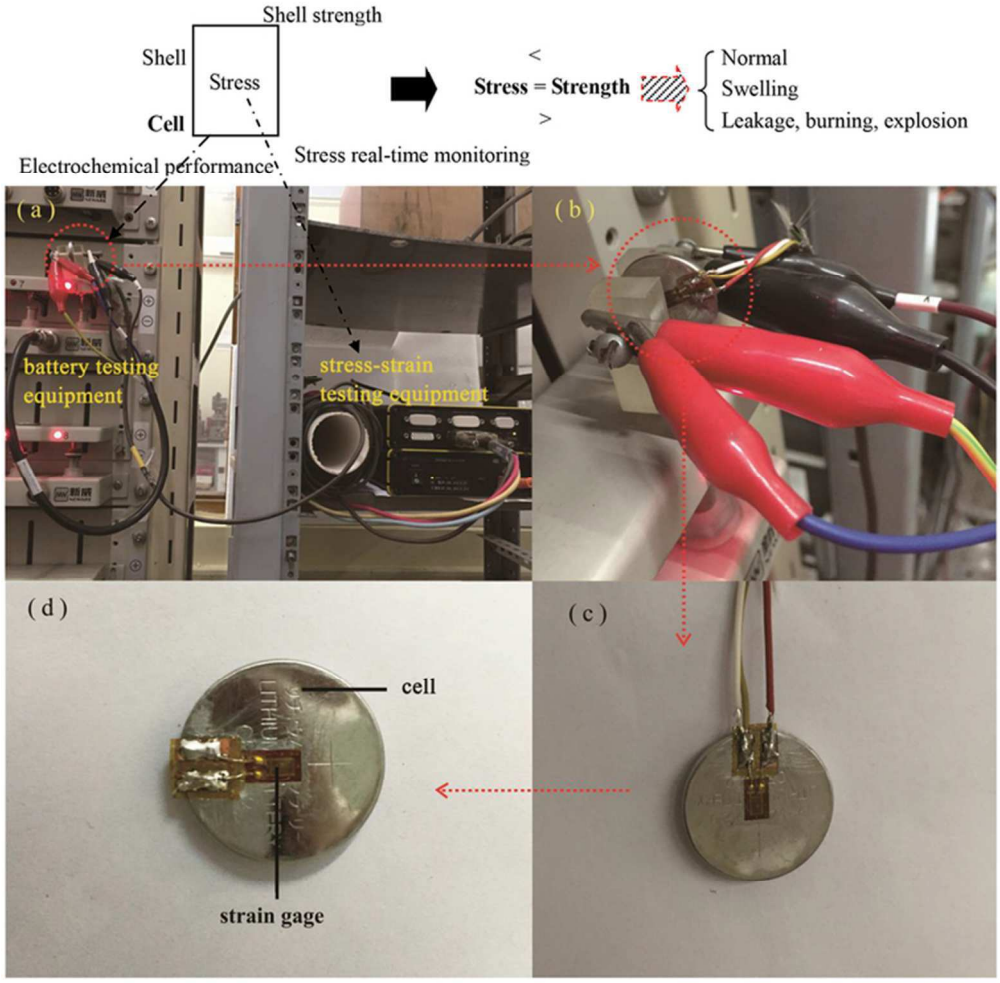

figure 1
64x64mm (300 x 300 DPI)

RSC Advances Accepted Manuscript

View Article Online
DOI: 10.1039/C6RA08774D

Published on 22 June 2016. Downloaded by Sichuan University on 24/06/2016 05:17:58.

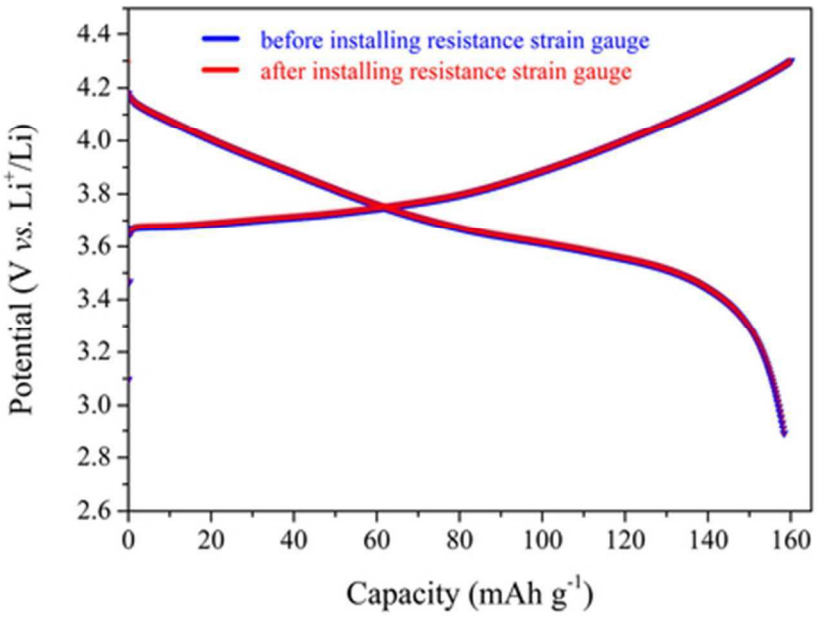

figure 2
44x31mm (300 x 300 DPI)

RSC Advances Accepted Manuscript

View Article Online
DOI: 10.1039/C6RA08774D

Published on 22 June 2016. Downloaded by Sichuan University on 24/06/2016 05:17:58.

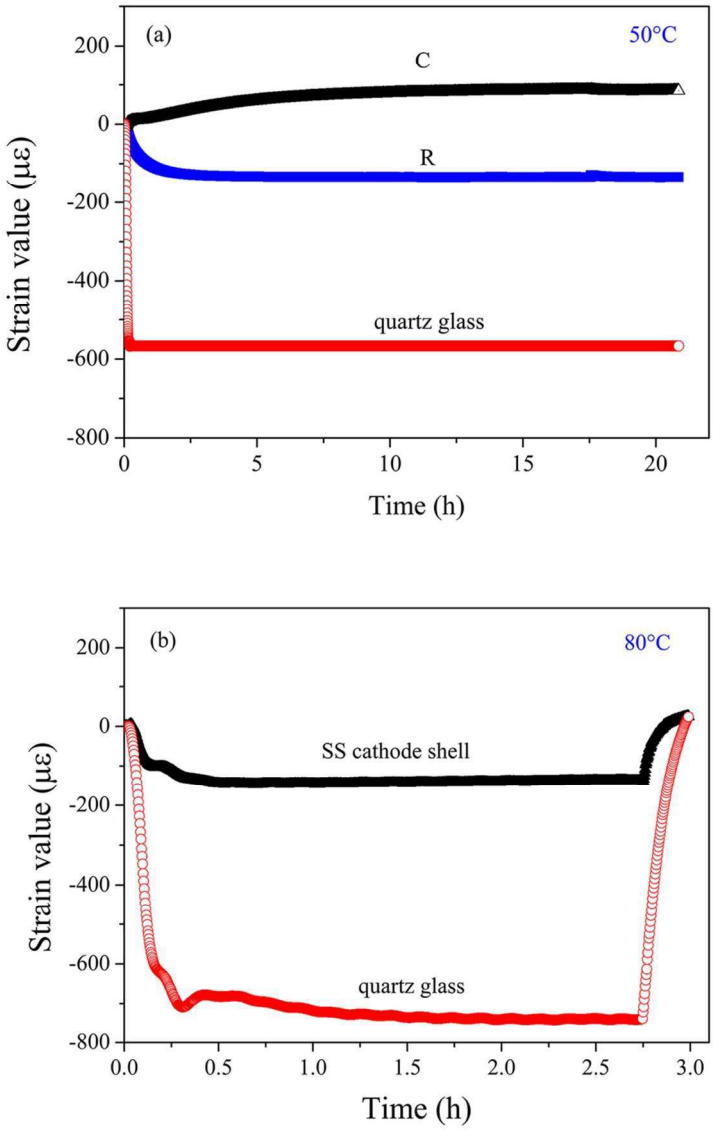

figure 3
88x124mm (300 x 300 DPI)

RSC Advances Accepted Manuscript

View Article Online
DOI: 10.1039/C6RA08774D

Published on 22 June 2016. Downloaded by Sichuan University on 24/06/2016 05:17:58.

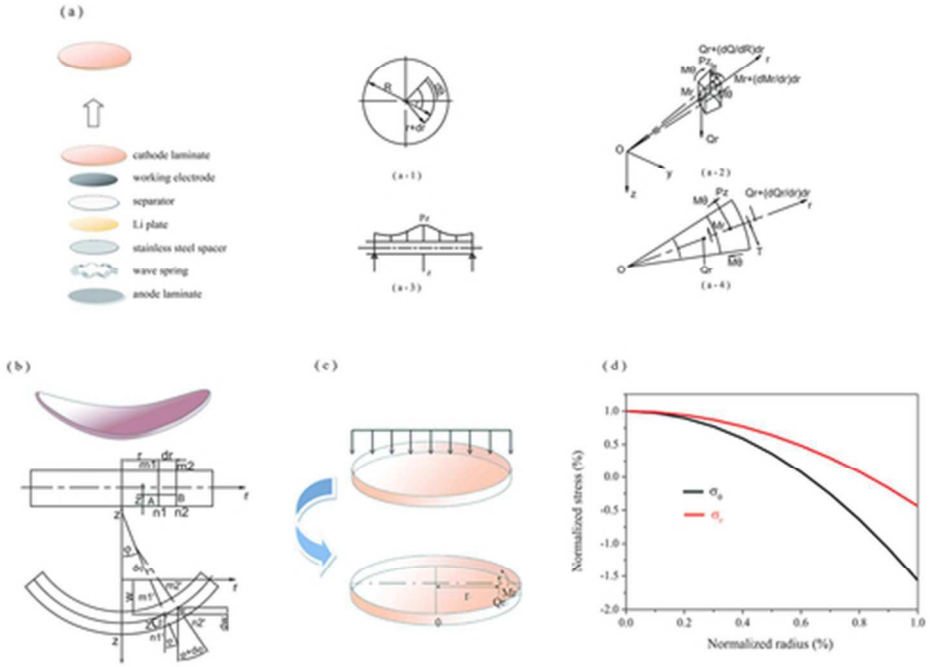

figure 4
44x31mm (300 x 300 DPI)

RSC Advances Accepted Manuscript

View Article Online
DOI: 10.1039/C6RA08774D

Published on 22 June 2016. Downloaded by Sichuan University on 24/06/2016 05:17:58.

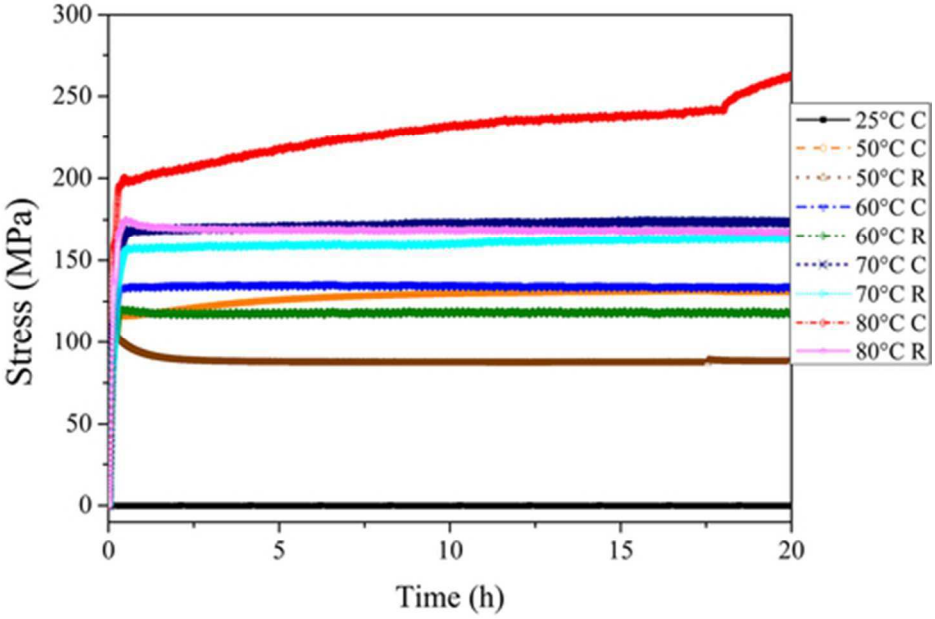

figure 5
44x31mm (300 x 300 DPI)

RSC Advances Accepted Manuscript

View Article Online
DOI: 10.1039/C6RA08774D

Published on 22 June 2016. Downloaded by Sichuan University on 24/06/2016 05:17:58.

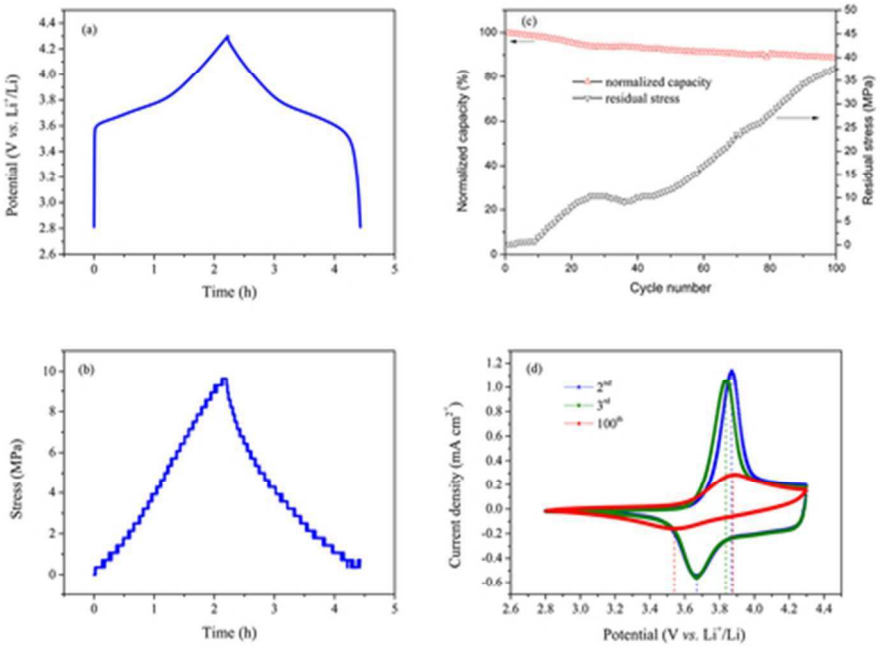

figure 6
45x32mm (300 x 300 DPI)

RSC Advances Accepted Manuscript

View Article Online
DOI: 10.1039/C6RA08774D

Published on 22 June 2016. Downloaded by Sichuan University on 24/06/2016 05:17:58.

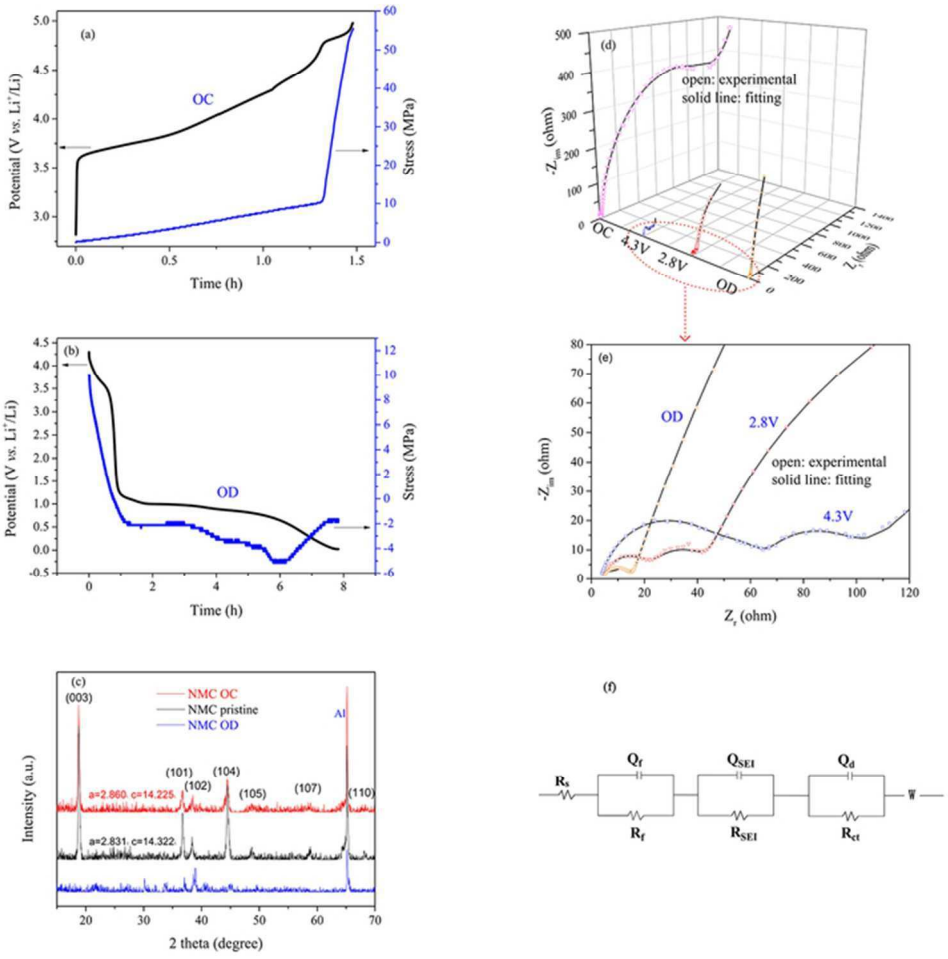

figure 7
63x64mm (300 x 300 DPI)

RSC Advances Accepted Manuscript

View Article Online
DOI: 10.1039/C6RA08774D

Published on 22 June 2016. Downloaded by Sichuan University on 24/06/2016 05:17:58.

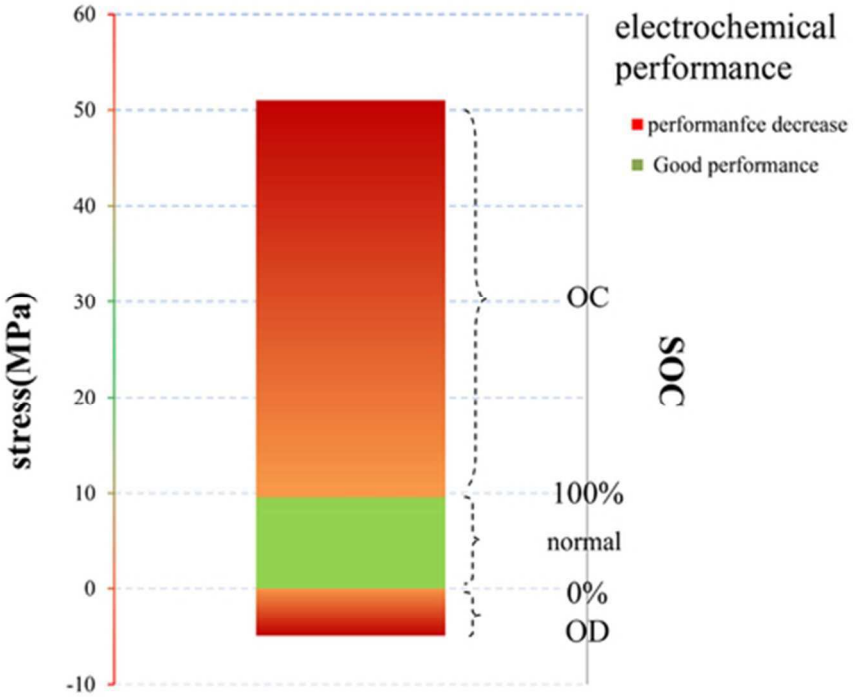

figure 8
47x35mm (300 x 300 DPI)

RSC Advances Accepted Manuscript

View Article Online
DOI: 10.1039/C6RA08774D

Graphical abstract:

The stresses in lithium cells are real-time monitored without destruction, and the relationship between stress and electrochemical performance is discussed.

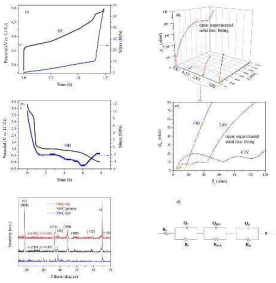

Published on 22 June 2016. Downloaded by Sichuan University on 24/06/2016 05:17:58.

RSC Advances Accepted Manuscript